The Role of Edge-Localized Neoclassical Tearing Modes in Quiescent H-mode Plasmas in the DIII-D Tokamak

Q.M. Hu[1,a)], R. Nazikian[2], X. Chen[2], Q. Yu[3], M. Austin[4], A. Bortolon[1], D. Ernst[5], S. Haskey[1], J.-K. Park[1], Z. Yan[6], G.Y. Yu[7]

[1] *Princeton Plasma Physics Laboratory, Princeton, NJ 08543-0451, USA*
[2] *General Atomics, P.O. Box 85608, San Diego, CA 92186-5608, USA*
[3] *Max-Plank-Institut fur Plasmaphysik, 85748 Garching, Germany*
[4] *The University of Texas at Austin, Austin, Texas 78712, USA*
[5] *Massachusetts Institute of Technology, Cambridge, MA, 02139, USA*
[6] *University of Wisconsin-Madison, Madison, Wisconsin 53706, USA*
[7] *University of California at Davis, CA 95616, USA,*
a) Author to whom correspondence should be addressed: qhu@pppl.gov

The edge-harmonic-oscillations (EHOs) in standard quiescent H-mode (QH-mode) plasmas in DIII-D are consistent with edge-localized neoclassical tearing modes (NTMs) based on non-linear two-fluid MHD simulations. Using kinetic equilibria constrained by edge profile measurements, the MHD simulations show that the $n = 1$ NTM and its harmonics can be destabilized at the pedestal-top of QH-mode plasma by the edge bootstrap current. The simulations further show that the unstable NTMs can saturate either at small (<2% ψ_N) or large (>4% ψ_N) island width depending on the magnitude of the edge bootstrap current, where ψ_N is the normalized radius in poloidal flux. The onset of the EHO also results in a prompt decrease in the pedestal width and height, consistent with simulation results for the onset of the NTM at the top of the QH-mode pedestal. This suggests that the avoidance of Edge Localized Modes (ELMs) in QH-mode can be attributed to the enhanced local transport induced by the NTM that is sufficient to prevent the expansion of the pedestal to an unstable width, analogous to the mechanism explored for ELM suppression by resonant magnetic perturbations. Nonlinear MHD simulations scanning the E×B frequency and the ratio of parallel and perpendicular thermal diffusivity ($\chi_{\parallel}/\chi_{\perp}$) at the pedestal top show that edge-localized NTMs are destabilized for conditions of high E×B frequency, high pedestal temperature and low pedestal density, qualitatively consistent with experimental conditions required for observing the EHO.

In toroidal plasma devices, a high confinement mode of plasma operation (H-mode) is often accompanied by edge-localized modes (ELMs) driven by the edge current and the high pressure gradient of the H-mode pedestal.[1] ELMs can release periodic bursts of heat and particles from the plasma,[1] which can enhance erosion and potentially damage plasma facing components. Consequently, elimination or mitigation of ELMs is necessary for fusion devices such as ITER.[1] One potential solution is quiescent H-mode (QH-mode),[2–10] which exhibits favorable H-mode confinement without ELMs. QH-mode operation is generally accompanied by a coherent edge-localized low-toroidal mode number (low-n) mode, called the edge harmonic oscillation (EHO).[11] EHOs mostly dominated by $n = 1$ mode and can be effective to maintain stationary H-mode conditions with the pedestal height and width remaining below the Peeling-Ballooning stability boundary.[12–17] Early experiments on the DIII-D tokamak investigated the hypothesis that EHO is a tearing mode, but no phase inversion around the mode rational surface is found in the density fluctuations.[11] The EHO is conjectured to be related to a saturated kink/peeling mode partially driven by the edge current and by sufficient E×B shear.[18–22] Detailed stability analysis of QH-mode plasmas in DIII-D reveals that the pedestal lies below the ideal low n kink/peeling stability boundary.[15,23] indicating that a better understanding of the triggering mechanism for EHO instability is required. Interestingly, locking of EHO sometimes happens in DIII-D,[24] which shows very similar dynamics to locking of core tearing mode.

In this letter, we show results from DIII-D experiments and non-linear MHD simulations indicating that the EHOs in QH-mode plasmas are remarkably consistent with narrow saturated neoclassical tearing mode (NTMs) driven by the edge bootstrap current. The predominant occurrence of EHOs in conditions of low pedestal density, high pedestal temperature and high edge E×B rotation is consistent with predictions from non-linear two-fluids MHD simulation for the conditions required to destabilize edge NTMs.

Time traces for a typical DIII-D QH-mode discharge 157102 are shown in Fig. 1. This discharge is used for comparison with modeling results in much of the discussion that follows. It is a neutral beam heated deuterium plasma with the toroidal magnetic field ($B_T \sim 2.06$ T), plasma current ($I_p \sim 1.1$ MA) in the B_T direction, 6.2 MW counter neutral beam injection, and edge safety factor of $q_{95} \sim 5.5$. Fig. 1 shows entry to QH-mode shortly after the LH transition at t~1.04s, which is concomitant by the appearance of the EHO with a growth time of ~30 ms. The pedestal density and temperature remain nearly stationary (Fig.1(d)) throughout the discharge with $n_{e,ped} \approx 1.1\times10^{19}$m^{-3}, $T_{e,ped} \approx 1.3$keV and pedestal electron collisionality $\upsilon_{*e} \sim 0.1$. The coherent EHO is dominated by an $m/n = 5/1$ mode measured by magnetic sensors (Fig. 1(b)). The mode is also seen on other measurements at the plasma edge.[16] There is a brief interval in the discharge, between 1.54 and 1.58 s, where the EHO vanishes following an ELM (indicated

by the large spike in the D_α signal (Fig. 1(a)), after which the EHO reappears with a growth time of ~30 ms until its saturation. The impact of the EHO on the pedestal is indicated by the drop in $n_{e,ped}$ and $T_{e,ped}$ (Fig. 1(d)), and changes in the density and temperature profiles (Fig. 4(a) and 3(b)) seen when the EHO reappears near 1.58 s. Statistical analysis of more than 600 EHO discharges dominated by n=1 mode shows that, for more than 80% of the discharges , the growth time of the EHO is about 20-50 ms. The growth time of EHO is much longer than the local resistive diffusion time (<1 ms) across the resistive layer in the pedestal, indicating the mode is tearing type.[25] In addition, the magnetic perturbation by EHO grows linearly instead of exponentially versus time, which is consistent with the growth characteristic of neoclassical tearing mode.[26]

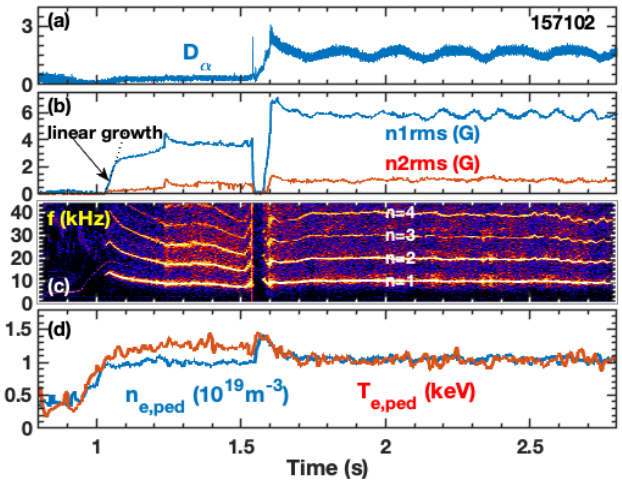

FIG. 1. Time evolution of standard QH plasma (157102) with n = 1 EHO, in terms of (a) D_α signal, (b) amplitude of n = 1 and 2 EHO magnetic perturbation, (c) Fourier analysis of the magnetic sensor signal and (d) pedestal density and temperature.

Kinetic theories indicate that, the stability of high-m NTMs is predominantly determined by the stabilizing Rutherford **Δ'** parameter, the destabilizing effect of the helically perturbed bootstrap current, and the destabilizing/stabilizing effect of the ion polarization current.[26–29] To explore NTM stability in QH-mode plasma, we use the two-fluid MHD code TM1,[30,31] with input parameters obtained from experimentally measured profiles, kinetically constrained equilibria and interpretive transport analysis using the TRANSP code.[32] These input parameters are: profiles of electron density n_e, electron temperature T_e, E×B rotation ($\omega_E = E_r/|RB_\theta|$, derived from measured toroidal rotation, poloidal rotation and ion diamagnetic drift), bootstrap current J_b derived from the measured n_e and T_e profiles based on Sauter's model, [33] and the safety factor q, effective charge Z_{eff}; the profiles of perpendicular particle ($D_\perp$), thermal ($\chi_\perp$), and momentum (χ_φ) diffusivities derived from TRANSP calculation, the details of these input parameters are listed in Table 1 of Ref. 34 TM1 is a nonlinear two-fluid MHD code based on the large aspect-ratio approximation with circular cross-section. TM1 self-consistently treats the Rutherford **Δ'** parameter and includes the effects of the bootstrap current, diamagnetic drifts and ion polarization current. Non-local, kinetic[35–37] and shaping effects,[38] are not included, however the TM1 code can be used to show qualitatively how edge NTMs can account for the phenomenology of the EHO and the parameter dependence of the QH-mode regime. Also, TM1 requires a seed island width for NTMs and such a seed can be provided by other MHD activity, i.e., such as kink/peeling modes, which are not excluded from playing a role in the EHO dynamics. TM1 has been used successfully to study core NTMs,[39–41] and to simulate magnetic island formation due to resonant magnetic perturbations (RMPs) and the modification of the pedestal height and width leading to ELM suppression.[34,42–44]

For the QH-mode plasma in Fig. 1, the input kinetic equilibrium profiles for TM1 are shown in Fig. 4 at ~1.57 s just before the onset of EHO activity and 30 ms after the ELM event. The TRANSP code[32] is used to estimate the thermal and particle diffusivities, plasma viscosity, collisionality, and resistivity at ~1.57 s, which are: $\chi_\varphi \approx \chi_e \approx 3D_\perp \approx 1.2\text{m}^2/\text{s}$ and neoclassical resistivity $\approx 1\times10^{-7}$ Ωm. $\chi_\parallel/\chi_\perp$ is of order 4×10^8 in these low collisionality plasmas.[30,45] These parameters are included as constraints in the TM1 simulations and parameter scans are performed to explore the stability boundary of the NTM on edge magnetic surfaces individually (m/n = 4/1, 5/1, 6/1, 9/2, 10/2, 11/2, etc). To make sure of good numerical convergence, a small radial grid size (1/3200 of the plasma minor radius) and time step ($\Delta t \leq 0.5\tau_A$, here τ_A is Alfven time) are used. The numerical convergence has been checked by varying the spatial resolution and time step by one order of magnitude.

Several thousand nonlinear simulations were performed in order to scan key drive parameters for NTMs in these QH-mode plasmas, including the edge bootstrap current and initial magnetic perturbation amplitude (seed island required for NTM). Here, an initial profile of m/n = 5/1 helical flux perturbation (and hence the initial seed island/magnetic perturbation) is implemented in the simulations. The 5/1 TM is stable when the bootstrap current is not included. We find that only the m/n = 5/1 NTM and its harmonics are unstable near the pedestal-top of the target plasma as illustrated in Fig. 2. The location of the 5/1 rational surface is shown in Fig. 4 and is aligned with the top of the pedestal. Fig. 2(a) shows the contour plot of the 5/1 saturated island width from TM1 versus bootstrap current (vertical axis) and seed island width W_0 (horizontal axis). Here, the normalized bootstrap current $J_{b,norm}$ is scanned from 0 to 1.5 times the experimental value obtained using the Sauter model,[33] while the q profile is kept unchanged to avoid the complexity of multiple variations. On the other hand, the shift in the resonant surface by the decay of the bootstrap current is very small compared to the island width. Fig. 2(a) shows that depending on the magnitude of the edge bootstrap current, the 5/1 NTM can be a) stable for $J_{b,norm}<0.35$, b) unstable with a small saturated island width $<2\%\psi_N$ for $0.35<J_{b,norm}<0.85$, and c) unstable with a larger saturated island width $>4\%\psi_N$ for $J_{b,norm}>0.85$. It is found that the small and large island regions correspond to drift tearing and NTM, respectively. Interestingly, the two separate saturation regions are also predicted for core 3/2 NTMs.[31] Fig. 2(c) shows the spectrogram of the simulated magnetic

perturbation due to the 5/1 NTM and its harmonics for the case p_3. The decreasing mode frequency during the mode growth is consistent with experiment.

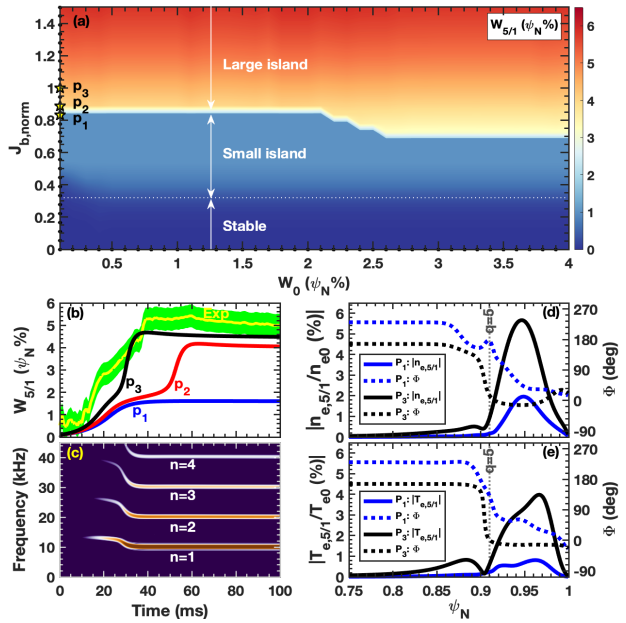

FIG. 2. TM1 simulation of 5/1 NTM stability by scanning the bootstrap current density ($J_{b,norm}$) and initial seed island width (W_0): (a) contour plot of the saturated 5/1 island width versus $J_{b,norm}$ and W_0, (b) time evolution of the 5/1 island width for p_1-p_3 points marked in (a) and overlaid with derived 5/1 island width from experiment in green band, and (c) Fourier analysis of the simulated magnetic perturbation associated with 5/1 NTM and its harmonics. Profiles of the amplitude (solid) and phase (dotted) of (d) temperature and (e) density fluctuation for p_1 (blue) and p_3 (black). Here, $J_{b,norm}$ is the bootstrap current normalized by J_b for shot 157102 at 1.57s, and the location of 5/1 surface is overlaid in (d-e).

Fig. 2(b) shows the time evolution of the TM1 simulated 5/1 island width for three different $J_{b,norm}$ marked by p_1-p_3 in Fig. 2(a). For a small initial seed island and a strong enough bootstrap current ($J_{b,norm}$>0.8), the NTM grows first to a small island and then further grows to large island, as illustrated by the 2 separate growth periods for the cases p_2 with $J_{b,norm}$=0.9 and p_3 with $J_{b,norm}$=1. The very weak seed perturbation can be generated easily by other MHD instabilities, i.e. edge kink/peeling mode. The time scale of the 5/1 mode growth is usually 20-60 ms depending on its initial state. For the experimental case with $J_{b,norm}$=1 (p_3), the 5/1 mode saturates at the width of 0.046ψ_N, which is close to the island width (0.05ψ_N) derived from the measured magnetic perturbations and equilibrium[46] as shown by the yellow curve. Here, the green band indicates 10% uncertainty in the inferred island width from magnetic measurements. The saturated island width is estimated to be ~2.5 cm at the outer midplane and ~5 cm in the flux expansion region at upper and lower 90 deg as shown in Fig. 3, and is larger than the ion banana width ~1 cm at the pedestal top. Here, the results in Fig. 3 are mapped from TM1 results in the flux surface coordinate and cylindrical geometry to the shaped poloidal cross-section based on the 2D equilibrium of shot 157102 at 1.57 s.

TM1 simulations show that the density and temperature fluctuations peak in the steep pedestal region as illustrated in Fig. 2(d-e) for the cases p_1 and p_3. The asymmetry of the fluctuations around the mode rational surface is consistent with the much larger gradient in density and temperature on the outboard side of the rational surface, in agreement with experimental observations of local EHO features showing dominant density and temperature fluctuations in the gradient region of the pedestal.[16] Diagnostic limitations and measurement artifacts [47,48] make it difficult to unambiguously identify the island induced inversion at the top of the pedestal, similar to that encountered in detecting small magnetic islands driven by RMPs in ELM suppressed plasmas.[34,49].

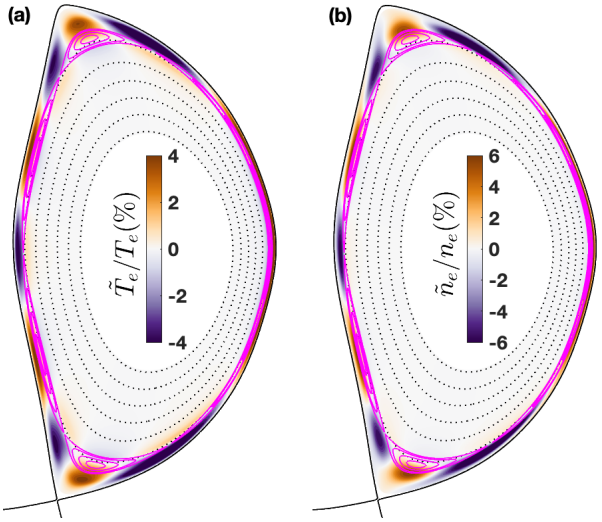

FIG. 3. 2D contour plot of the simulated (a) temperature and (b) density fluctuations in the shaped poloidal cross-section overlaid with the 5/1 island in magenta. Here, the TM1 results in the flux surface coordinate and cylindrical geometry are mapped to the shaped poloidal cross-section based on the 2D equilibrium of shot 157102 at 1.57 s.

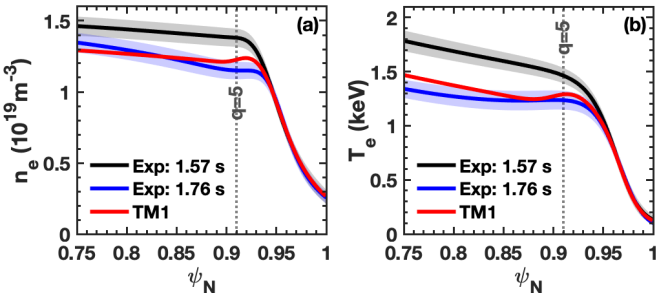

FIG. 4. Comparison of the profiles of (a) n_e and (b) T_e, between experiment at 1.76 s (blue) and TM1 simulation (red) at p_3 marked in Fig.2(a). Here, the initial profiles of n_e and T_e at 1.57 s are shown in black dotted curves in (a) and (b). The bands show the uncertainties of the fitted profiles for the measured n_e and T_e.

Fig. 4 shows the comparison of the measured (a) density and (b) temperature profiles (black curves) at 1.57 s just before the onset of the EHO and at 1.76 s after the mode saturates and profiles relax (blue curves). Also shown is the TM1 simulated profiles for case p_3 after the NTM saturation at 100 ms in Fig.

2b. We find that the growth of the 5/1 NTM degrades the density and temperature pedestal height and width, and also flattens the initially non-flat profiles at the top of the pedestal, consistent with experimental observations as shown in Fig. 4. This flattening results in a narrowing of the pedestal width as seen in the change of profiles. The reduction in the pedestal height and width by the NTM is also similar to the effect observed for RMP driven magnetic islands in ELM suppressed plasmas.[34] Thus, a common picture is emerging that edge magnetic islands (either driven by RMPs or others) prevent the expansion of the pedestal to an unstable width, thereby suppressing ELMs.

Experiments in DIII-D frequently show that increasing the density or decreasing the NBI torque (that decreases the E×B frequency at the pedestal top) leads to a vanishing of the EHO [50] as shown in Fig.4. Here, we choose discharges with similar plasma parameters to Fig. 1 and perform a density and torque (E×B rotation) scan to identify the stability boundary for the EHO. For shot 163467 (red curves) in Fig. 5, the initially saturated n = 1 EHO begins to vanish at 2 s as the pedestal density increases from 1×10^{19} m^{-3} to 2×10^{19} m^{-3}. The pedestal temperature (not shown) does not vary significantly and is close to 1.2keV during the entire period. ELMs appear as the EHO decays, as shown in Fig. 5d. For the second shot 157092, the saturated n = 1 EHO disappears at 2.8 s (blue curves in Fig. 5) as the NBI torque is reduced.

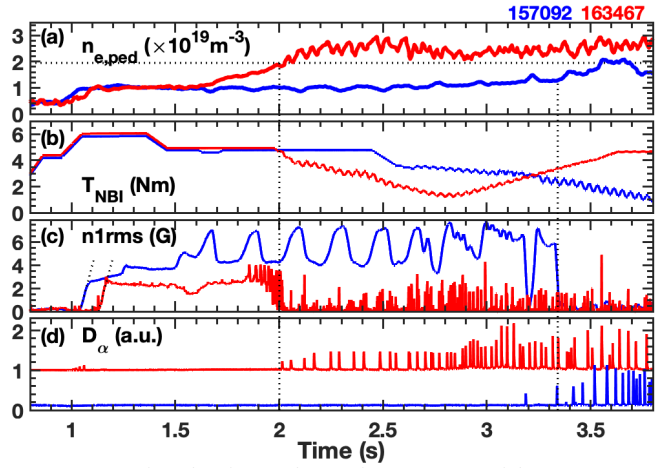

FIG. 5. Increasing density or decreasing torque vanishes n=1 EHO, in terms of time evolution of (a) pedestal density, (b) NBI torque, (c) amplitude of n=1 EHO magnetic perturbation and (d) Dα for shots 157092 and 163467.

We find a similar sensitivity of the edge NTM to density and E×B rotation as observed in experiment during the density and torque ramp, respectively. Fig. 6(a) shows the simulated 5/1 island width (color contours) versus $J_{b,norm}$ and E×B frequency ($\omega_E = E_r/|RB_\theta|$) using an initial seed island width W_0 = 0.01ψ_N. We keep the equilibrium profiles and transport coefficients fixed for illustration purposes. Here, the global profile of E×B frequency is proportionally scanned, and $\omega_{E,norm}$ denotes the scanned E×B frequency at the 5/1 surface normalized to the experimental value. The 5/1 NTM is stabilized at low E×B frequency ($\omega_{E,norm}$<0.6). For $\omega_{E,norm}$>0.8, depending on the amplitude of edge bootstrap current, the 5/1 NTM is unstable and saturates to either the small (<2 %ψ_N) or larger (>4%ψ_N) island size. The saturated island width for shot 157102 is denoted by the yellow star in Fig. 6(a) and clearly resides in the large island width region, but not too far away from the boundary between the large and small island region.

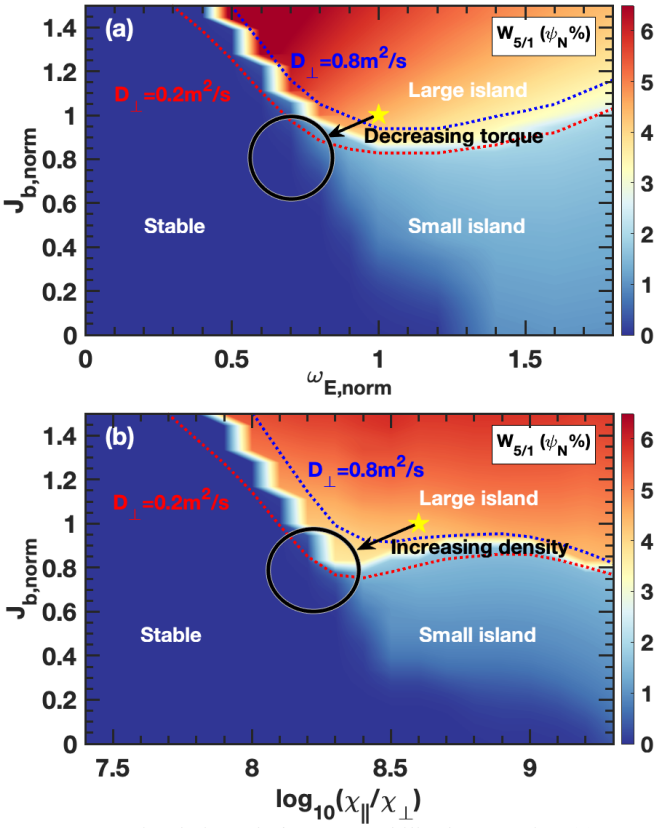

FIG. 6. TM1 simulation of 5/1 NTM stability by scanning (a) $J_{b,norm}$ versus the E×B frequency and (b) $J_{b,norm}$ versus ratio of $\chi_\parallel/\chi_\perp$ in terms of contour plot the saturated 5/1 island width. The blue and red dotted curves indicate the stability boundary of the large NTM with half and double the D$\perp$. Here, W_0 = 0.01 ψ_N is used, $\omega_{E,norm}$ is the E×B frequency normalized by the experimental value at 1.57 s. The yellow star indicates the experimental parameter for shot 157102.

The destabilizing effect on the NTM associated with increasing $\omega_{E,norm}$ can be understood from the modified Rutherford equation.[26] The ion polarization current term, which is proportional to $-(\omega-\omega_E)(\omega-\omega_E-\omega_{*e})/W^3$,[26,27,35,50] is found to decrease since the value of $(\omega-\omega_E)(\omega-\omega_E-\omega_{*e})$ decreases by more than 4 times in the simulations when scanning $\omega_{E,norm}$ from 0 to 1.5. Here, ω, ω_{*e} and W are the mode frequency, the electron diamagnetic drift frequency and the magnetic island width. The change in the mode frequency is found to be correlated with the change in the eigenfunction, the increasing $\omega_{E,norm}$ leads to wider distribution of eigenfunction. Consequently, when increasing $\omega_{E,norm}$, the stabilizing effect of polarization current term becomes weaker, which together with Δ' ($\sim -2m/r$) can be overcome by the destabilizing effect of bootstrap current loss. As the E×B

rotation decreases at the pedestal top, the initial unstable point (yellow star in Fig. 6a) moves to the stable region denoted by the arrow and the circle region. It should be noted that the simulated tendency in Fig. 6(a) is different to analytical theory,[26,35] which assumes that changing the E×B rotation won't change the NTM stability. We think the reason is probably due to the strong asymmetry in the profile gradient on the two sides of the rational surface at the pedestal-top, compared to the constant gradient assumption in analytical theory.

The TM1 simulations also show that the edge NTM stability is sensitive to the pedestal density and temperature. Fig. 6(b) shows the TM1 simulation of the 5/1 island width versus $J_{b,norm}$ and the ratio of parallel and perpendicular thermal diffusivity ($\chi_\parallel/\chi_\perp$) using an initial seed island width $W_0 = 0.01\psi_N$. The shot 157102 is also shown by the yellow star. Here, $\chi_\parallel=\chi_{\parallel c}[1+(3.165\upsilon_{te}k_\parallel/\nu_e)^2]^{-0.5}$,[51] and $\chi_{\parallel c}=3.16\upsilon^2_{te}/\nu_e$ is the classical parallel electron heat conductivity, $k_\parallel=\boldsymbol{B}_0\cdot\boldsymbol{k}/|\boldsymbol{B}_0|$, υ_{te} is the electron thermal velocity and ν_e is the electron collisionality. $\chi_\parallel$ reduces to $\chi_{\parallel c}\propto T_e^{5/2}/n_e$ in collisional plasma with $\nu_e \gg \upsilon_{te}k_\parallel$, and to $\upsilon_{te}/k_\parallel\propto T_e^{0.5}$ in the collisionless limit. In the simulations, $\chi_\parallel$ is scanned from collisional to collisionless limit while $\chi_\perp$ is kept constant at the value obtained from TRANSP analysis. The figure shows that the 5/1 NTM is stabilized as the parallel transport decreases, which happens for increasing density or decreasing temperature. It should be noted that the measured Z_{eff} is about 5 in this QH discharge, which is much higher than Z_{eff}~1.5-2 in ELMing H-mode plasma and resulting in higher collisionality. The simulated results in Fig. 6(b) can be understood as follows: at higher density and lower temperature the parallel transport weakens, leading to weaker bootstrap current loss (less destabilizing effect), hence making the 5/1 NTM more stable at higher n_e and lower T_e. The simulation results in Fig. 6(b) are qualitatively consistent with experimental observations in shot 157092 (red curves in Fig. 5). In the experiment the factor of two increase in the pedestal density leads to a 50% decrease in $\chi_\parallel/\chi_\perp$. This change is sufficient to move the 5/1 NTM into the stable region as indicated by the arrow to the black circle region in Fig. 6(b).

It should be noted that NTM stability is sensitive to the uncertainty in the transport coefficients, and we address this uncertainty through additional non-linear scans. TRANSP analysis indicates an uncertainty of $D_\perp$ in the range of 0.3-0.7m^2/s, and weaker uncertainty of χ_φ and χ_e in the range of ~1.2±0.2m^2/s. Accordingly, the TM1 simulation scans are repeated for $D_\perp$=0.2 and 0.8m^2/s values at the top of the pedestal and the results are shown in Fig. 6. We overlay the boundary of the unstable large island region for the case of the lower $D_\perp$ (red dotted curve) and the higher $D_\perp$ (blue dotted curve). The shift in the boundary of the large island saturation region is minor, indicating that the sensitivity to the uncertainty in $D_\perp$ is weak.

Practical implications of our simulation results are that the EHOs can be characterized by nonlinear edge-localized NTMs. Decreasing the E×B rotation, the pedestal temperature, or increasing the pedestal density are found to be stabilizing for the edge-localized NTM in our simulations, as seen in experiments. The saturated NTM island width, mode frequency and pedestal regulation from TM1 simulations are consistent with experimental observations for QH-modes plasmas with EHOs. Our simulations indicate that edge NTM causes peaking in the density and temperature fluctuations in the steep pedestal region instead of inside the island, which is consistent with experimental observations but different to the characterization of core NTM. The sharp ~180 deg phase transition in the fluctuations around the pedestal-top with a much weaker fluctuation magnitude challenges recent diagnostics to verify the nature of the EHO, which may be resolved by better diagnostics with higher spatial resolution. Further studies are also needed to explore the broader parameter space of pedestal conditions for the appearance of NTMs, including q_{95}, plasma shape effects, and conditions for the prevalence of n = 1 versus higher-n (n = 2, 3) EHOs compared to NTM predictions. Improved nonlinear models including non-local, kinetic and shaping effects will further enhance the accuracy of these predictions and better resolve the phenomena that give rise to QH-mode conditions.

ACKNOWLEDGEMENTS

The authors greatly appreciate Dr. K.H. Burrell for many helpful discussions. This material is based upon work supported by the U.S. Department of Energy, Office of Science, Office of Fusion Energy Sciences, using the DIII-D National Fusion Facility, a DOE Office of Science user facility, under Awards No. DE-AC02-09CH11466, No. DE-FC02-04ER54698, No. DE-SC0014264, No. DE-FG02-08ER54999, No. DE-FG02-97ER54415, and No. DE-FG02-99ER54531.

REFERENCES

[1] A. Loarte, B. Lipschultz, A.S. Kukushkin, G.F. Matthews, P.C. Stangeby, N. Asakura, G.F. Counsell, G. Federici, A. Kallenbach, K. Krieger, A. Mahdavi, V. Philipps, D. Reiter, J. Roth, J. Strachan, D. Whyte, R. Doerner, T. Eich, W. Fundamenski, A. Herrmann, M. Fenstermacher, P. Ghendrih, M. Groth, A. Kirschner, S. Konoshima, B. LaBombard, P. Lang, A.W. Leonard, P. Monier-Garbet, R. Neu, H. Pacher, B. Pegourie, R.A. Pitts, S. Takamura, J. Terry, E. Tsitrone, and the ITPA Scrape-off Layer and Divertor Physics Topical Group, Nucl. Fusion **47**, S203 (2007).

[2] K.H. Burrell, M.E. Austin, D.P. Brennan, J.C. DeBoo, E.J. Doyle, C. Fenzi, C. Fuchs, P. Gohil, C.M. Greenfield, R.J. Groebner, L.L. Lao, T.C. Luce, M.A. Makowski, G.R. McKee, R.A. Moyer, C.C. Petty, M. Porkolab, C.L. Rettig, T.L. Rhodes, J.C. Rost, B.W. Stallard, E.J. Strait, E.J. Synakowski, M.R. Wade, J.G. Watkins, and W.P. West, Phys. Plasmas **8**, 2153 (2001).

[3] W. Suttrop, M. Maraschek, G.D. Conway, H.-U. Fahrbach, G. Haas, L.D. Horton, T. Kurki-Suonio, C.J. Lasnier, A.W. Leonard, C.F. Maggi, H. Meister, A.M. ck, R. Neu, I. Nunes, T.P. tterich, M. Reich, A.C.C. Sips, and the A.U. Team, Plasma Phys. Control. Fusion **45**, 1399 (2003).

[4] N. Oyama, Y. Sakamoto, A. Isayama, M. Takechi, P. Gohil, L.L. Lao, P.B. Snyder, T. Fujita, S. Ide, Y. Kamada, Y. Miura, T. Oikawa, T. Suzuki, H. Takenaga, K. Toi, and the J.-60 Team, Nucl. Fusion **45**, 871 (2005).

[5] K.H. Burrell, T.H. Osborne, P.B. Snyder, W.P. West, M.E.

Fenstermacher, R.J. Groebner, P. Gohil, A.W. Leonard, and W.M. Solomon, Phys. Rev. Lett. **102**, 155003 (2009).
[6] A.M. Garofalo, W.M. Solomon, J.-K. Park, K.H. Burrell, J.C. DeBoo, M.J. Lanctot, G.R. McKee, H. Reimerdes, L. Schmitz, M.J. Schaffer, and P.B. Snyder, Nucl. Fusion **51**, 083018 (2011).
[7] W.M. Solomon, P.B. Snyder, K.H. Burrell, M.E. Fenstermacher, A.M. Garofalo, B.A. Grierson, A. Loarte, G.R. McKee, R. Nazikian, and T.H. Osborne, Phys. Rev. Lett. **113**, 135001 (2014).
[8] X. Chen, K.H. Burrell, T.H. Osborne, W.M. Solomon, K. Barada, A.M. Garofalo, R.J. Groebner, N.C. Luhmann, G.R. McKee, C.M. Muscatello, M. Ono, C.C. Petty, M. Porkolab, T.L. Rhodes, J.C. Rost, P.B. Snyder, G.M. Staebler, B.J. Tobias, and Z.Y. and, Nucl. Fusion **57**, 022007 (2016).
[9] K. Barada, T.L. Rhodes, K.H. Burrell, L. Zeng, L. Bardóczi, X. Chen, C.M. Muscatello, and W.A. Peebles, Phys. Rev. Lett. **120**, 135002 (2018).
[10] E. Viezzer, Nucl. Fusion **58**, 115002 (2018).
[11] K.H. Burrell, M.E. Austin, D.P. Brennan, J.C. DeBoo, E.J. Doyle, P. Gohil, C.M. Greenfield, R.J. Groebner, L.L. Lao, T.C. Luce, M.A. Makowski, G.R. McKee, R.A. Moyer, T.H. Osborne, M. Porkolab, T.L. Rhodes, J.C. Rost, M.J. Schaffer, B.W. Stallard, E.J. Strait, M.R. Wade, G. Wang, J.G. Watkins, W.P. West, and L. Zeng, Plasma Phys. Control. Fusion **44**, A253 (2002).
[12] B.A. Grierson, K.H. Burrell, R.M. Nazikian, W.M. Solomon, A.M. Garofalo, E.A. Belli, G.M. Staebler, M.E. Fenstermacher, G.R. McKee, T.E. Evans, D.M. Orlov, S.P. Smith, C. Chrobak, and C. Chrystal, Phys. Plasmas **22**, 055901 (2015).
[13] K.H. Burrell, W.P. West, E.J. Doyle, M.E. Austin, T.A. Casper, P. Gohil, C.M. Greenfield, R.J. Groebner, A.W. Hyatt, R.J. Jayakumar, D.H. Kaplan, L.L. Lao, A.W. Leonard, M.A. Makowski, G.R. McKee, T.H. Osborne, P.B. Snyder, W.M. Solomon, D.M. Thomas, T.L. Rhodes, E.J. Strait, M.R. Wade, G. Wang, and L. Zeng, Phys. Plasmas **12**, 056121 (2005).
[14] T.H. Osborne, P.B. Snyder, K.H. Burrell, T.E. Evans, M.E. Fenstermacher, A.W. Leonard, R.A. Moyer, M.J. Schaffer, and W.P. West, J. Phys.: Conf. Ser. **123**, 012014 (2008).
[15] K.H. Burrell, T.H. Osborne, P.B. Snyder, W.P. West, M.E. Fenstermacher, R.J. Groebner, P. Gohil, A.W. Leonard, and W.M. Solomon, Nucl. Fusion **49**, 085024 (2009).
[16] X. Chen, K.H. Burrell, N.M. Ferraro, T.H. Osborne, M.E. Austin, A.M. Garofalo, R.J. Groebner, G.J. Kramer, N.C. Luhmann, G.R. McKee, C.M. Muscatello, R. Nazikian, X. Ren, P.B. Snyder, W.M. Solomon, B.J. Tobias, and Z. Yan, Nucl. Fusion **56**, 076011 (2016).
[17] K. Kamiya, K. Itoh, N. Aiba, N. Oyama, M. Honda, and A. Isayama, Commun. Phys. **4**, 1 (2021).
[18] P.B. Snyder, K.H. Burrell, H.R. Wilson, M.S. Chu, M.E. Fenstermacher, A.W. Leonard, R.A. Moyer, T.H. Osborne, M. Umansky, W.P. West, and X.Q. Xu, Nucl. Fusion **47**, 961 (2007).
[19] D. Brunetti, J.P. Graves, E. Lazzaro, A. Mariani, S. Nowak, W.A. Cooper, and C. Wahlberg, Phys. Rev. Lett. **122**, 155003 (2019).
[20] F. Liu, G.T.A. Huijsmans, A. Loarte, A.M. Garofalo, W.M. Solomon, P.B. Snyder, M. Hoelzl, and L. Zeng, Nucl. Fusion **55**, 113002 (2015).
[21] A.M. Garofalo, K.H. Burrell, D. Eldon, B.A. Grierson, J.M. Hanson, C. Holland, G.T.A. Huijsmans, F. Liu, A. Loarte, O. Meneghini, T.H. Osborne, C. Paz-Soldan, S.P. Smith, P.B. Snyder, W.M. Solomon, A.D. Turnbull, and L. Zeng, Phys. Plasmas **22**, 056116 (2015).
[22] J.R. King, K.H. Burrell, A.M. Garofalo, R.J. Groebner, S.E. Kruger, A.Y. Pankin, and P.B. Snyder, Nucl. Fusion **57**, 022002 (2016).
[23] W.P. West, K.H. Burrell, T.A. Casper, E.J. Doyle, P.B. Snyder, P. Gohil, L.L. Lao, C.J. Lasnier, A.W. Leonard, M.F.F. Nave, T.H. Osborne, D.M. Thomas, G. Wang, and L. Zeng, Nucl. Fusion **45**, 1708 (2005).
[24] K.H. Burrell, A.M. Garofalo, W.M. Solomon, M.E. Fenstermacher, D.M. Orlov, T.H. Osborne, J.-K. Park, and P.B. Snyder, Nucl. Fusion **53**, 073038 (2013).
[25] Q. Yu, S. Günter, K. Lackner, and M. Maraschek, Nucl. Fusion **52**, 063020 (2012).
[26] R.J. La Haye, Phys. Plasmas **13**, 055501 (2006).
[27] H.R. Wilson, J.W. Connor, R.J. Hastie, and C.C. Hegna, Phys. Plasmas **3**, 248 (1996).
[28] O. Sauter, R.J. La Haye, Z. Chang, D.A. Gates, Y. Kamada, H. Zohm, A. Bondeson, D. Boucher, J.D. Callen, M.S. Chu, T.A. Gianakon, O. Gruber, R.W. Harvey, C.C. Hegna, L.L. Lao, D.A. Monticello, F. Perkins, A. Pletzer, A.H. Reiman, M. Rosenbluth, E.J. Strait, T.S. Taylor, A.D. Turnbull, F. Waelbroeck, J.C. Wesley, H.R. Wilson, and R. Yoshino, Phys. Plasmas **4**, 1654 (1997).
[29] R. Fitzpatrick, F.L. Waelbroeck, and F. Militello, Phys. Plasmas **13**, 122507 (2006).
[30] Q. Yu, S. Günter, and B.D. Scott, Phys. Plasmas **10**, 797 (2003).
[31] Q. Yu, Nucl. Fusion **50**, 025014 (2010).
[32] J. Breslau, M. Gorelenkova, F. Poli, J. Sachdev, and X. Yuan, (2018).
[33] O. Sauter, C. Angioni, and Y.R. Lin-Liu, Phys. Plasmas **6**, 2834 (1999).
[34] Q.M. Hu, R. Nazikian, B.A. Grierson, N.C. Logan, C. Paz-Soldan, and Q. Yu, Nucl. Fusion **60**, 076001 (2020).
[35] F.L. Waelbroeck, J.W. Connor, and H.R. Wilson, Phys. Rev. Lett. **87**, 215003 (2001).
[36] E. Poli, A. Bergmann, and A.G. Peeters, Phys. Rev. Lett. **94**, 205001 (2005).
[37] K. Imada, H.R. Wilson, J.W. Connor, A.V. Dudkovskaia, and P. Hill, Phys. Rev. Lett. **121**, 175001 (2018).
[38] A.H. Glasser, J.M. Greene, and J.L. Johnson, The Physics of Fluids **18**, 875 (1975).
[39] Q. Yu, S. Günter, and K. Lackner, Phys. Plasmas **11**, 140 (2003).
[40] Q. Yu and S. Günter, Nucl. Fusion **48**, 065004 (2008).
[41] Q. Yu, Nucl. Fusion **60**, 084001 (2020).
[42] Q.M. Hu, R. Nazikian, B.A. Grierson, N.C. Logan, J.-K. Park, C. Paz-Soldan, and Q. Yu, Phys. Plasmas **26**, 120702 (2019).
[43] Q.M. Hu, R. Nazikian, B.A. Grierson, N.C. Logan, D.M. Orlov, C. Paz-Soldan, and Q. Yu, Phys. Rev. Lett. **125**, 045001 (2020).
[44] Q.M. Hu, R. Nazikian, N.C. Logan, J.-K. Park, C. Paz-Soldan, S.M. Yang, B.A. Grierson, Y. In, Y.M. Jeon, M. Kim, S.K. Kim, D.M. Orlov, G.Y. Park, and Q. Yu, Phys. Plasmas **28**, 052505 (2021).
[45] Z. Chang and J.D. Callen, Physics of Fluids B: Plasma Physics **4**, 1167 (1992).
[46] W.W. Heidbrink, L. Bardoczi, C.S. Collins, G.J. Kramer, R.J.L. Haye, D.J. Lin, C.M. Muscatello, M. Podestà, L. Stagner, M.A.V. Zeeland, and Y.B. Zhu, Nucl. Fusion **58**, 082027 (2018).
[47] G. McKee, R. Ashley, R. Durst, R. Fonck, M. Jakubowski, K. Tritz, K. Burrell, C. Greenfield, and J. Robinson, Rev. Sci. Instrum. **70**, 913 (1999).
[48] G. Yu, R. Nazikian, Y. Zhu, Y. Zheng, G. Kramer, A. Diallo, Z. Li, X. Chen, D. Ernst, Y. Zheng, M. Austin, and N.C.L. Jr, Plasma Phys. Control. Fusion **64**, 095014 (2022).
[49] R. Nazikian, C. Paz-Soldan, J.D. Callen, J.S. deGrassie, D. Eldon, T.E. Evans, N.M. Ferraro, B.A. Grierson, R.J. Groebner, S.R. Haskey, C.C. Hegna, J.D. King, N.C. Logan, G.R. McKee, R.A. Moyer, M. Okabayashi, D.M. Orlov, T.H. Osborne, J.-K. Park, T.L. Rhodes, M.W. Shafer, P.B. Snyder, W.M. Solomon, E.J. Strait, and M.R. Wade, Phys. Rev. Lett. **114**, 105002 (2015).
[50] K.H. Burrell, K. Barada, X. Chen, A.M. Garofalo, R.J. Groebner, C.M. Muscatello, T.H. Osborne, C.C. Petty, T.L. Rhodes, P.B. Snyder, W.M. Solomon, Z. Yan, and L. Zeng, Phys. Plasmas **23**,

056103 (2016).
[51] F.L. Hinton and R.D. Hazeltine, Rev. Mod. Phys. **48**, 239 (1976).